Title
JACOBIAN FREE GLOBAL EVENT ANALYSIS

Authors
Danielewicz, P.
Gyulassy, M.

Publication Date
1983-02-01

Lawrence Berkeley Laboratory
UNIVERSITY OF CALIFORNIA

Submitted to Physics Letters B

JACOBIAN FREE GLOBAL EVENT ANALYSIS

P. Danielewicz and M. Gyulassy

February 1983

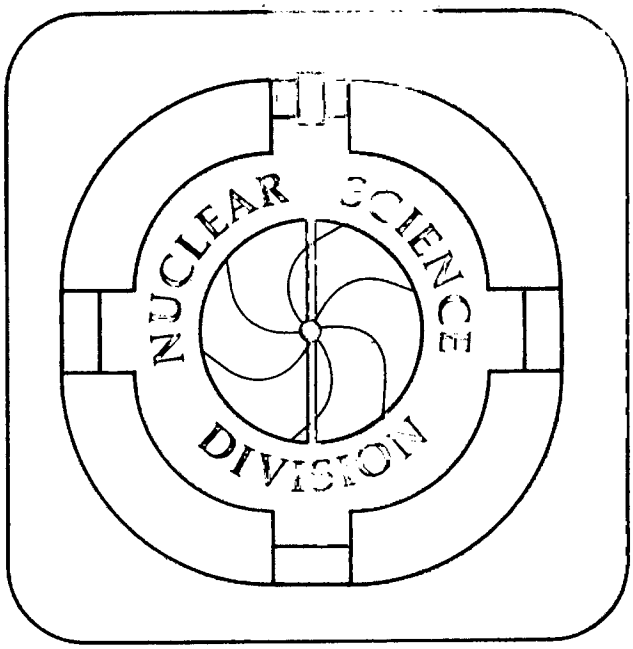

Prepared for the U.S. Department of Energy under Contract DE-AC03-76SF00098

DISCLAIMER

DISCLAIMER

JACOBIAN FREE GLOBAL EVENT ANALYSIS*

P. DANIELEWICZ† and M. GYULASSY

Nuclear Science Division
Lawrence Berkeley Laboratory
University of California
Berkeley, CA 94720

Abstract

Conventional global event analysis using the sphericity tensor is shown to be biased against shapes with degenerate radii and vanishing flow angles for multiplicities M < 100. The Jacobian responsible for that bias is computed analytically. We construct a Jacobian free distribution that eliminates most of the $O(1/\sqrt{M})$ distortions. Finally, an azimuthally corrected sphericity matrix is shown to be useful in searching for collective flow phenomena in nuclear collisions.

The general sphericity matrix [1-3] is given by

$$S_{ij} = \sum_{\nu=1}^{M} \omega_\nu p_i(\nu) p_j(\nu) \quad , \tag{1}$$

where i,j = 1,2,3 refer to a Cartesian coordinate system with the 3-axis pointed along the beam direction, and ω_ν are scalar weight factors. Measurement of S requires the determination of the momenta $\underset{\sim}{p}(\nu)$ of M particles in each event. Therefore, S measures global properties of the reaction. Interest has focused recently on global analysis in the area of nuclear collisions [2-9] because of its promise in searching for collective flow phenomena [10].

*Work supported by the Director, Office of Energy Research, Division of Nuclear Physics of the Office of High Energy and Nuclear Physics of the U.S. Department of Energy under Contract DE-AC03-76SF00098.

†On leave of absence from Institute of Theoretical Physics, Warsaw University, Warsaw, Poland.

In this letter, we show, however, that conventional sphericity analysis does not provide accurate event shape determination for multiplicities $M < 100$. The source of the distortions is identified as a Jacobian factor reflecting the true phase space density of eigenvalues and rotation angles of S. We show that dividing the distribution function of eigenvalues by that Jacobian eliminates most of the distortion to order $1/\sqrt{M}$ and leads to a more model-independent event shape analysis. We begin by computing the distribution function of sphericity matrix elements as a function of multiplicity. Numerical examples based on Monte Carlo sampling of general Gaussian distributions illustrate our points.

Given an M particle inclusive distribution ρ_M normalized to unity, the joint probability density to find the matrix elements of S between T_{ij} and $T_{ij} + dT_{ij}$ is

$$\Phi_M(T) = \int d^3\underset{\sim}{p}(1) \ldots d^3\underset{\sim}{p}(M)\ \rho_M(\underset{\sim}{p}(1), \ldots, \underset{\sim}{p}(M)) \prod_{i\geq j} \delta(S_{ij} - T_{ij}) \quad . \tag{2}$$

The average value of S_{ij} depends, however, only on the single-particle inclusive distribution ρ_1

$$\langle S_{ij} \rangle = M \int d^3p\ p_i p_j \rho_1(p) \equiv M \langle p_i p_j \rangle \quad . \tag{3}$$

We assume henceforth that $\omega_\nu = 1$ for simplicity*. In the limit $M \to \infty$, the central limit theorem assures us that $\Phi_M(T_N)$ will be of Gaussian form and a strongly peaked function around $T_{ij} = \langle S_{ij} \rangle$. Therefore, what eq. (2) reveals are the finite number fluctuations around those average values.

---

*The Jacobian we compute (eq. (6)) and the numerical results with the generalized Gaussian model (eq. (9)) are independent of ω_ν.

Since S_{ij} provides basically a measurement of the second moments of the single-particle inclusive distribution $\rho_1(\underset{\sim}{p})$, it is important to recall why we need to measure all M particle momenta in the first place. The answer is that any single-particle measurement necessarily averages over the azimuthal angle, ϕ, of the reaction plane. Therefore, only the ϕ-averaged sphericity moments can be determined via single-particle inclusive distributions. Note that by measuring $\rho_1(p)$ associated with multiplicity cuts [7,8] we can eliminate much of the impact parameter averaging; i.e., a narrow range of partial waves can be isolated. However, multiplicity triggers cannot eliminate the average over ϕ. This loss of information is restored only via global event analysis. By studying the distribution of sphericity matrices, the ϕ averaging can be circumvented, and the true three-dimensional event structure can be revealed.

The geometrical content of S is exhibited by diagonalizing it as follows:

$$S = \Lambda F \Lambda^{+} \quad , \tag{4}$$

where $F = \text{diag}\,(f_1, f_2, f_3)$ is the diagonal matrix of eigenvalues ordered such that $0 \leq f_1 \leq f_2 \leq f_3$ and

$$\Lambda = R_z(\phi)\, R_y(\theta)\, R_z(\chi) \tag{5}$$

is a product of the orthogonal rotation matrices about the fixed z, y, and z axes with angles χ, θ, and ϕ, respectively. Clearly (θ,ϕ) are the polar and azimuthal angles of the eigenvector, $e_3 = \Lambda e_z$, associated with the largest eigenvalue; f_3. Physically, θ corresponds to the angle of most rapid collective matter flow, while ϕ is an estimate of the azimuthal angle of the reaction plane. The next most rapid collective flow is oriented along $e_2 = \Lambda e_y$, while the slowest collective flow is along $e_1 = e_3 \times e_2$ with our convention. Because S is symmetric the event shape is assumed to be symmetric

under space inversion. Therefore, S characterizes an event in momentum space as an oriented ellipsoid with principal axes along e_i and radii $\sqrt{f_i}$.

Since ϕ is not under our control, we are interested not in $\Phi_M(S_{ij})$, but rather in the distribution, $d^6P_M/df_1df_2df_3d\theta d\phi dX$, of eigenvalues and rotation angles. However, transforming variables from S_{ij} to (f_i,θ,ϕ,X) necessarily brings in a Jacobian factor

$$J(f_i,\theta) = \left| \frac{\partial^6[\Lambda F\Lambda^+]}{\partial^6[f_i,\theta,\phi,X]} \right|$$

$$= \sin\theta\,(f_3 - f_1)(f_3 - f_2)(f_2 - f_1)$$

$$\equiv \sin\theta\, J(f_i) \quad , \tag{6}$$

so that

$$\frac{d^6P_M}{df_1df_2df_3d\theta d\phi dX} = \Phi_M(\Lambda F\Lambda^+)\, J(f_i) \sin\theta \quad . \tag{7}$$

Note that P_M is normalized such that

$$\int_0^\infty df_3 \int_0^{f_3} df_2 \int_0^{f_2} df_1 \int_0^{\pi/2} d\theta \int_{-\pi}^{\pi} d\phi \int_0^{\pi} dX d^6P_M = 1 \quad . \tag{8}$$

Equation (6) can be verified by direct algebra. The occurrence of the Vandermonde determinant, $J(f_i)$, of eigenvalues of symmetric matrices is a result known from the theory of random matrices [11]. This combination of eigenvalues follows from dimensional analysis and the nonexistence of the inverse transformation when two or more eigenvalues are the same. Geometrically, the Jacobian simply reflects the fact that the number of ellipsoids with degenerate radii is much smaller than the number with nonequal radii. Physically, J has the effect of suppressing very strongly event shapes close to a sphere, a cigar or a pancake.

Thus, even though Φ_M peaks strongly for $M \gg 1$ around the true averages, eq. (3), the peak of d^6P_M will be shifted by order $1/\sqrt{M}$ from the true eigenvalues for near degenerate cases. Although that shift is only $O(1/\sqrt{M})$, we show below that it is surprisingly large for multiplicities $M < 100$. The $\sin\theta$ factor induces a similar shift of the peak in the flow angle when it is close to 0. Note also that when evaluating average quantities such as $\langle\theta\rangle$ and $\langle f_3/f_1\rangle$, there is an additional distortion of order $1/\sqrt{M}$ because polar angles are limited to positive values and f_3 is enforced to be greater than f_1.

The finite multiplicity distortions of average flow quantities are shown in fig. 1. The curves were obtained via Monte Carlo evaluation of $\langle\theta\rangle$ and $\langle f_3/f_1\rangle$ for different multiplicities M as a function of an assumed value of $r_{31} = f_3/f_1$ and an orientation $\theta = 0$. Specifically, we sampled M momenta from the general uncorrelated Gaussian form

$$\rho_M \propto \exp[-M/2 \text{ Tr } SS_{th}^{-1}] \quad , \tag{9}$$

with $S_{th} = R_y(\theta_{th})F_{th}R_y(\theta_{th})$ and $F_{th} = \text{diag}(1,1,r_{31})$. From the M momenta so generated S was computed and diagonalized to obtain the $(f_i^{obs}, \theta^{obs}, \phi^{obs}, \chi^{obs})$ data. This process was repeated 1000 times to obtain $\langle\theta^{obs}\rangle$ and $\langle f_3^{obs}/f_1^{obs}\rangle$ for various assumed r_{31} and $\theta_{th} = 0$.

For the cigar shape with $r_{31} = 2$ and $\theta_{th} = 0$ in the theoretical distribution, we see from fig. 1 that for multiplicity $M = 10$, $\langle\theta^{obs}\rangle \approx 33°$, and $\langle f_3^{obs}/f_1^{obs}\rangle \approx 6.1$! For a theoretical sphere, $r_{31} = 1$, $\langle\theta^{obs}\rangle \approx 57°$, as required by symmetry, but $\langle f_3^{obs}/f_1^{obs}\rangle \approx 4.8$, 2.8, 2.0, and 1.5 for $M = 10$, 20, 40, and 100, respectively. For the pancake shape with $r_{31} = 2/3$, $\theta_{th} = 0$ (corresponding to $f_3/f_1 = f_2/f_1 = 3/2$, $\theta_{th} = 90°$), $\langle\theta^{obs}\rangle \approx 68°$, $\langle f_3^{obs}/f_1^{obs}\rangle \approx 5.2$ for $M = 10$. We see that the average flow characteristics of the shapes of greatest theoretical interest [3] are significantly distorted.

Figure 1 also shows the results of intranuclear cascade calculations [3] for Ne + Ne, Ar + Ar, and U + U collisions at 250 A MeV. The striking feature to note is that for Ne and Ar the points lie very close to the curves corresponding to zero flow angle! In particular, Ar + Ar does not even reach a spherical shape at b = 0. On the other hand, U does reach the spherical shape at b = 0, and there is a nonvanishing flow angle for intermediate impact parameters. Thus, even though the Ar and U results seem to coincide for intermediate impact parameters in the flow diagram [3], the conclusions about whether these nuclei flow differ because of the finite multiplicity distortions.

Simple analytic formulas can be obtained in special cases. For the uncorrelated Gaussian distribution, eq. (9), Φ_M is given by

$$\Phi_M(\Lambda F \Lambda^+) \propto e^{-\frac{M}{2}\,\mathrm{Tr}(\Lambda F \Lambda^+ S_{th}^{-1})} (\det F)^{\frac{M}{2}-2} . \tag{10}$$

Note that for $M \gg 1$, $\Phi_M \propto \exp[-M/4\ \mathrm{Tr}\ \delta S^2]$ is indeed of Gaussian form with $\delta S = \Lambda F \Lambda^+ S_{th}^{-1} - 1$. Equation (10) is obtained by noting that the exponential factor, eq. (9), can be pulled out of the integral because S is replaced by T. Next, changing variables from $p(\nu)$ to $\Lambda^{-1}p(\nu)$ for all ν and noting that the Jacobian $|\partial^6(\Lambda T \Lambda^{-1})/\partial^6(T)| = 1$, the product of delta functions is transformed to $\delta(S_{11} - f_1)\delta(S_{22} - f_2)\delta(S_{33} - f_3)\delta(S_{12})\delta(S_{13})\delta(S_{23})$. Changing finally to dimensionless variables $p_i(\nu)/\sqrt{f_i}$, we obtain $(\det F)^{M/2-2}$ times a constant dependent only on M (which is of no interest here).

For a Gaussian sphere, $S_{th} = 1$, eq. (10) reduces to

$$\Phi_M(\Lambda F \Lambda^{-1}) \propto \exp\left\{-\frac{M}{2}\sum_{i=1}^{3}\left[f_i - \left(1 - \frac{4}{M}\right)\ell n\ f_i\right]\right\} , \tag{11}$$

which indeed maximizes when $f_1 = f_2 = f_3$. However, the maximum of P_M is shifted by $O(1/\sqrt{M})$. A simple fit to our numerical results for $M \geq 20$ gives

$$\langle f_3^{obs}/f_1^{obs}\rangle \approx 1 + 3/\sqrt{M} + 22/M \quad . \tag{12}$$

Given a Gaussian distribution, eq. (9), the average sphericity matrix elements from eq. (3) are simply $\langle S_{ij}\rangle = S_{ij}^{th}$ and the variance of the matrix elements decreases with M as

$$\left[\langle S_{ij}^2\rangle - \langle S_{ij}\rangle^2\right]^{1/2} = \frac{1}{\sqrt{M}}\left(S_{ii}^{th}S_{jj}^{th} + (S_{ij}^{th})^2\right)^{1/2} \quad . \tag{13}$$

With eq. (13) an asymptotic formula for $\langle\theta_{obs}\rangle$ can be obtained for cigar shapes $f_1 = f_2$, $f_3 = r_{31}f_1$ by noting that $\langle S_{xz}^2 + S_{yz}^2\rangle \approx \langle\theta^2(f_3 - f_1)^2\rangle$ for $\theta << \pi/2$. Therefore, $\langle\theta_{obs}\rangle \simeq 57^\circ(2r_{31}/M)^{1/2}/(r_{31} - 1)$. This shows that angular distortions are significant either for small M or for r_{31} close to unity.

We have seen that the simple method of global analysis proposed in refs. [2,3] suffer from large finite multiplicity distortions. An obvious way to eliminate the order $1/\sqrt{M}$ distortions is to divide the measured d^6P_M in eq. (7) by $J(f_i,\theta)$ and search for maxima of d^6P_M/J. However, in practice enormous numbers of events would have to be measured to locate maxima of such a six-dimensional distribution. Therefore, practical considerations force us to consider one- and two-dimensional projections of ϕ_M.

Consider, in particular, the double differential distribution of aspect ratios $r_{32} = f_3/f_2$, $r_{21} = f_2/f_1$,

$$\frac{d^2N}{dr_{32}dr_{21}} = \int df_1df_2df_3\ \delta(r_{32} - f_3/f_2)\ \delta(r_{21} - f_2/f_1)\ \frac{d^3P_M}{df_1df_2df_3}$$

$$= \frac{r_{21}}{(1+r_{21}+r_{21}r_{32})^3}\int_0^\infty E^2dE\ \frac{d^3P_M}{df_1df_2df_3} \quad , \tag{14}$$

where in the last line d^3P_M is evaluated at f_i such that $E = \Sigma f_i$, $r_{21} = f_2/f_1$, $r_{32} = f_3/f_2$. The reason we chose (r_{32},r_{21}) rather than (r_{31},r_{21}) above is that

both r_{32} and r_{21} have a range 1 to ∞. Because d^3P_M includes the Jacobian $J(f_i)$ from eq. (6),

$$J(f_i) = \frac{E^3 r_{21}(r_{32}-1)(r_{21}-1)(r_{32}r_{21}-1)}{(1+r_{21}+r_{21}r_{32})^3} , \tag{15}$$

d^2N must vanish along the lines $r_{32} = 1$ and $r_{21} = 1$. This is illustrated in fig. 2a,c,e. These figures were obtained by performing the integration over E,θ,ϕ,χ in eq. (14) via the Monte Carlo Metropolis algorithm for d^6P_M given by eqs. (7,10).

It is now clear that, except for the dimensional E^3 factor in eq. (15), we can eliminate the bulk of the distortion in d^2N by defining a "corrected" distribution

$$\frac{d^2\mathcal{N}}{dr_{32}dr_{21}} = \frac{(1+r_{21}+r_{21}r_{23})^6}{r_{21}^2(r_{32}-1)(r_{21}-1)(r_{32}r_{21}-1)} \frac{d^2N}{dr_{32}dr_{21}} . \tag{16}$$

The dimensionless weight function in eq. (16) arises because we divide by the basic Vandermonde Jacobian, eq. (15), as well as the Jacobian in eq. (14) stemming from our choice of variables.

The corrected distributions are illustrated in fig. 2b,d,f. Note that unlike d^2N, the peak of $d^2\mathcal{N}$ is much closer to the input theoretical ratios. In particular, the sphere, cigar, and pancake shapes are immediately resolved by searching for the maximum of $d^2\mathcal{N}$. There is one important caveat, however. For any fixed multiplicity M there is a critical value, r_{crit}, of the aspect ratio r_{31} below which $d^2\mathcal{N}$ peaks at $r_{32} = r_{21} = 1$. For M = 20, 40, 80, we find that $r_{crit} \approx 1.8$, 1.5, and 1.3. For $r_{31} < r_{crit}(M)$, shape resolution is lost.

Consider next the distribution, $dN/d\cos\theta$, of flow angles. In fig. 3a we show the results obtained by Monte Carlo integration for an assumed cigar shape $r_{31} = 1.9$, $r_{21} = 1.0$ oriented at 20° with respect to the 3-axis. For $M = 100$, $dN/d\cos\theta$ clearly peaks at the correct angle. For $M < 40$, however, $dN/d\cos\theta$ peaks below 20°, and $M \lesssim 20$, $dN/d\cos\theta$ maximizes at 0°. (Of course, $dN/d\theta$ always peaks away from $\theta = 0$).

The ability to resolve a finite flow angle θ_{th} depends strongly on M and r_{31}. Figure 1 gives a qualitative guide to the angular resolution for fixed M and r_{31}. The curves for fixed M correspond to the flow angle fluctuations about $\theta = 0$ for a given r_{31}. It is clear that we cannot resolve flow angles that are much smaller than $\sim\langle\theta\rangle/2$ because polar angles must be positive. Since the sign of θ is kept track of only via ϕ, which we sum over, $dN/d\cos\theta$ is effectively the sum of two distributions, one corresponding to positive θ (i.e., $|\phi| < \pi/2$) and the other to negative θ (i.e., $\pi/2 < |\phi| < \pi$). When the true flow angle is less than $\sim\langle\theta\rangle/2$, these two contributions add such that the peak of $dN/d\cos\theta$ occurs near $\theta = 0$. It is important to emphasize that the only true signature of collective flow is a clear maximum of $dN/d\cos\theta$ away from $\theta = 0$. Average quantities such as $\langle\theta\rangle$ are strongly distorted by finite multiplicity fluctuations.

As a final handle on the finite multiplicity distortions, we consider event shape analysis in the rotated frame where $\phi = 0$. That frame varies, of course, from event to event. For large r_{31}, θ, and M it is clear that ϕ fluctuates about the true azimuthal angle of the reaction plane. Not knowing the reaction plane, we can approximate its azimuthal angle by ϕ itself. Consider now the average of the sphericity matrix rotated by $-\phi$ about the z axis

$$\langle S'_{ij}\rangle = \langle R_z(-\phi)\ S\ R_z(\phi)\rangle_{ij} = M\langle R_z(-\phi)_{ii'}\ R_z(-\phi)_{jj'} p_{i'} p_{j'}\rangle \quad . \qquad (17)$$

This average, unlike eq. (3), depends on the full M particle distribution because it requires knowledge of $\phi(\underset{\sim}{p}_1, \ldots, \underset{\sim}{p}_M)$. Diagonalizing $\langle S' \rangle$ we obtain a polar angle θ' and eigenvalue f'_i. Figure 3b shows θ' versus $r'_{32} = f'_3/f'_2$ for M = 40 for a variety of cigar shapes and orientations. The sphere is located at $\theta' = 57^\circ$ and an aspect ratio r'_{32} given approximately by

$$r'_{32} \approx 1 + 2.7/\sqrt{M} \quad . \tag{18}$$

As a function of M the grid pattern shifts so that the sphere point follows eq. (18). The most important feature to note in fig. 3b is that this phi-rotated aspect ratio is much less distorted than the unrotated r_{31} ratio in fig. 1. For M = 40, $r_{32} \gtrsim 1.5$ can be easily resolved. Furthermore, the angular distortion is also far less for the theoretically interesting range [3] $1.5 < r_{32} < 2.5$. Analysis in terms of θ' and r'_{32} is therefore useful when only a limited number of events can be measured [7,8]. Differential distributions such as $d^2N/dr_{32}dr_{21}$ and $dN/d\cos\theta$ require high statistics [9]. What fig. 3b shows is that for realistic multiplicities, M ~ 50, a significant reduction in distortion is possible by averaging phi-rotated sphericity matrices and then calculating θ' versus r'_{32}.

We conclude that in searching for collective flow effects the role of finite multiplicity distortions for $M \lesssim 100$ needs special attention. The simplest reduction of such distortions is achieved by the ϕ-rotated analysis in terms of θ' and r'_{32}. However, confirmation of true flow angle requires a maximum of $dN/d\cos\theta$. When high enough statistics are available, then the Jacobian free distribution, $d^2\mathcal{N}/dr_{32}dr_{21}$, provides the most distortion-free shape information.

Acknowledgments:

We are grateful to H.G. Ritter, D. Beavis, and W. Swiatecki for many stimulating discussions. We also acknowledge the Gesellschaft für Schwerionenforschung for making their computer facilities available to us. This work was supported by the Director, Office of Energy Research, Division of Nuclear Physics of the Office of High Energy and Nuclear Physics of the U.S. Department of Energy under Contract DE-AC03-76SF00098.

References

[1] S.L. Wu and G. Zobernig, Z. Phys. C2 (1979) 107.

[2] J. Cugnon et al, Phys. Lett. 109B (1982) 167.

[3] M. Gyulassy et al, Phys. Lett. 110B (1982) 185.

[4] J. Cugnon and D. L'Hote, CEN Saclay preprint (1982).

[5] J. Kapusta and D. Strottmann, Phys. Rev. C23 (1981) 1282.

[6] H. Stöcker et al., Phys. Rev. C25 (1982) 1873.

[7] H. Stroebele et al., GSI-82-32 preprint (1982).

[8] D. Beavis et al., UC Riverside preprint (1982).

[9] H.G. Ritter, in Proc. 3rd Intl. Conf. on Nuclear Reaction Mechanisms, ed. E. Gadioli (Varenna, Italy, June 1982) p. 682;
H.H. Gutbrod et al. in Proc. Intl. Conf. on Nucleus-Nucleus Collisions (Michigan State University, Michigan, 1982), LBL-14980 preprint, Nucl. Phys. A, in press.

[10] H. Stöcker et al., Phys. Lett. 103B (1981) 269.

[11] A. Bohr and B.R. Mottelson, Nuclear Structure, Vol. 1, p. 298 (W.A. Benjamin, Inc., 1969, New York, Amsterdam).

Figure Captions

Fig. 1. The average polar angle and aspect ratio f_3/f_1 for events sampled from eq. (9) with different multiplicities M and aspect ratios r_{31} and $\theta_{th} = 0$. The sphere is mapped onto the $\langle\theta\rangle = 57^\circ$ line with $\langle f_3/f_1\rangle$ given by eq. (12). The diamonds, triangles, and dots correspond to the intranuclear calculations of ref. [3] for Ne + Ne, Ar + Ar, U + U at 250A MeV, respectively. Note that only U collisions involve finite flow angles.

Fig. 2. (a,c,e) Double differential distribution of aspect ratios $r_{32} = f_3/f_2$ and $r_{21} = f_2/f_1$ with $d^2N/dr_{32}dr_{21}$ given by eq. (14). (b,d,f) The Jacobian free $d^2\mathcal{N}/dr_{32}dr_{21}$ given by eq. (16). Contours show relative intensity for sphere (a,b), cigar with $r_{31} = 1.9$ (c,d), and pancake with $r_{31} = 1.9$ (e,f).

Fig. 3. a) Differential distribution of $\cos\theta$ plotted versus θ for a cigar shape $r_{31} = 1.9$ oriented at $\theta = 20^\circ$. The dependence on multiplicity M is illustrated.

b) Polar angle θ' and aspect ratio f'_3/f'_2 obtained by diagonalizing the average ϕ-rotated sphericity matrix, eq. (17). The grid illustrates how the theoretical rectangular grid in θ_{th} and r_{32} is distorted for M = 40. The sphere point follows eq. (18). Note that the interesting region [3] for nuclear collisions $1.5 < r_{32} < 2.5$ is much less distorted in this diagram than in fig. 1.

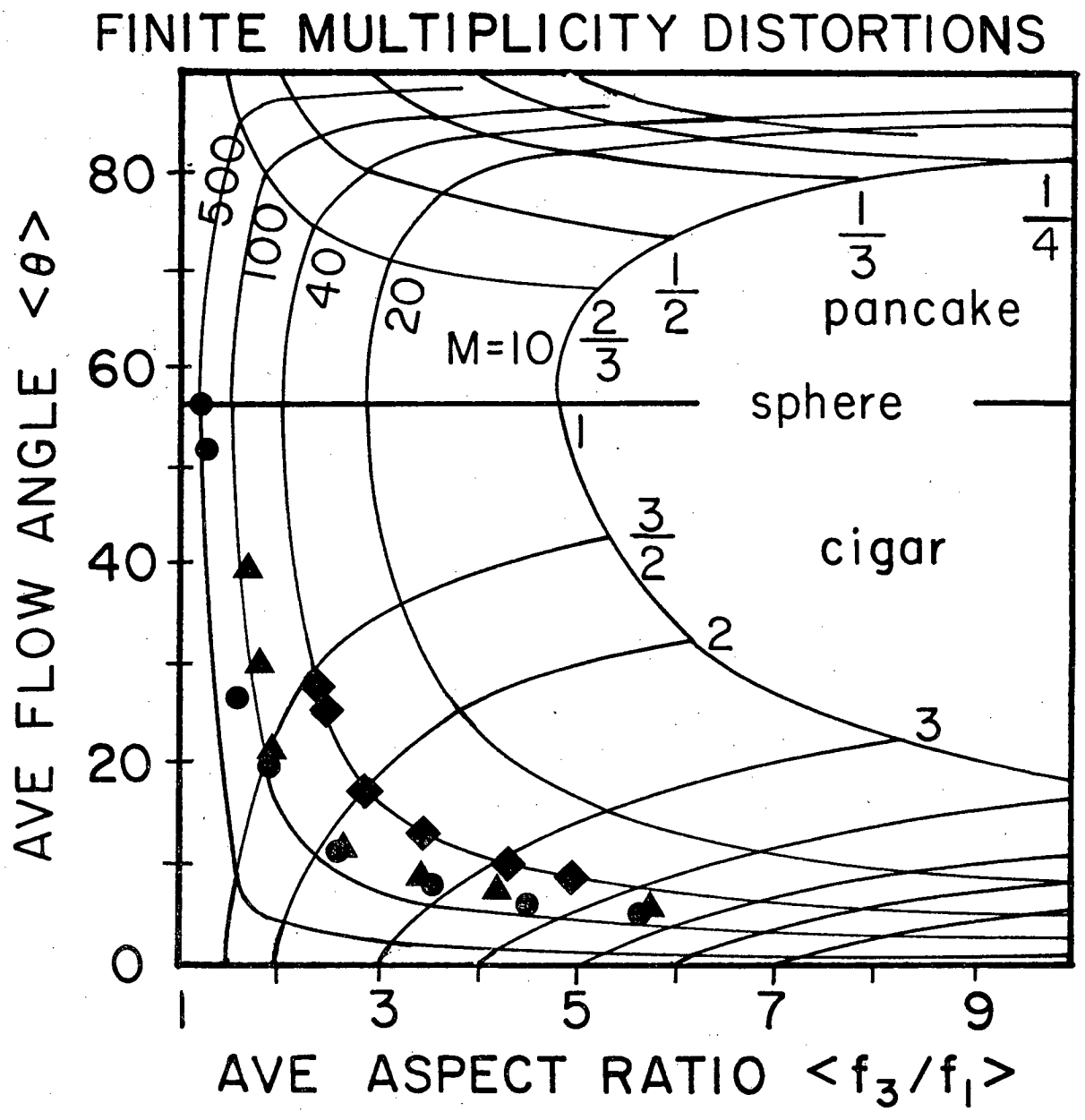
FINITE MULTIPLICITY DISTORTIONS
AVE FLOW ANGLE <θ>
AVE ASPECT RATIO <f3/f1>
0
20
40
60
80
1
3
5
7
9
500
100
40
20
M=10
2/3
1/2
1/3
1/4
pancake
sphere
1
3/2
2
3
cigar
XBL 832-8003

Fig. 1

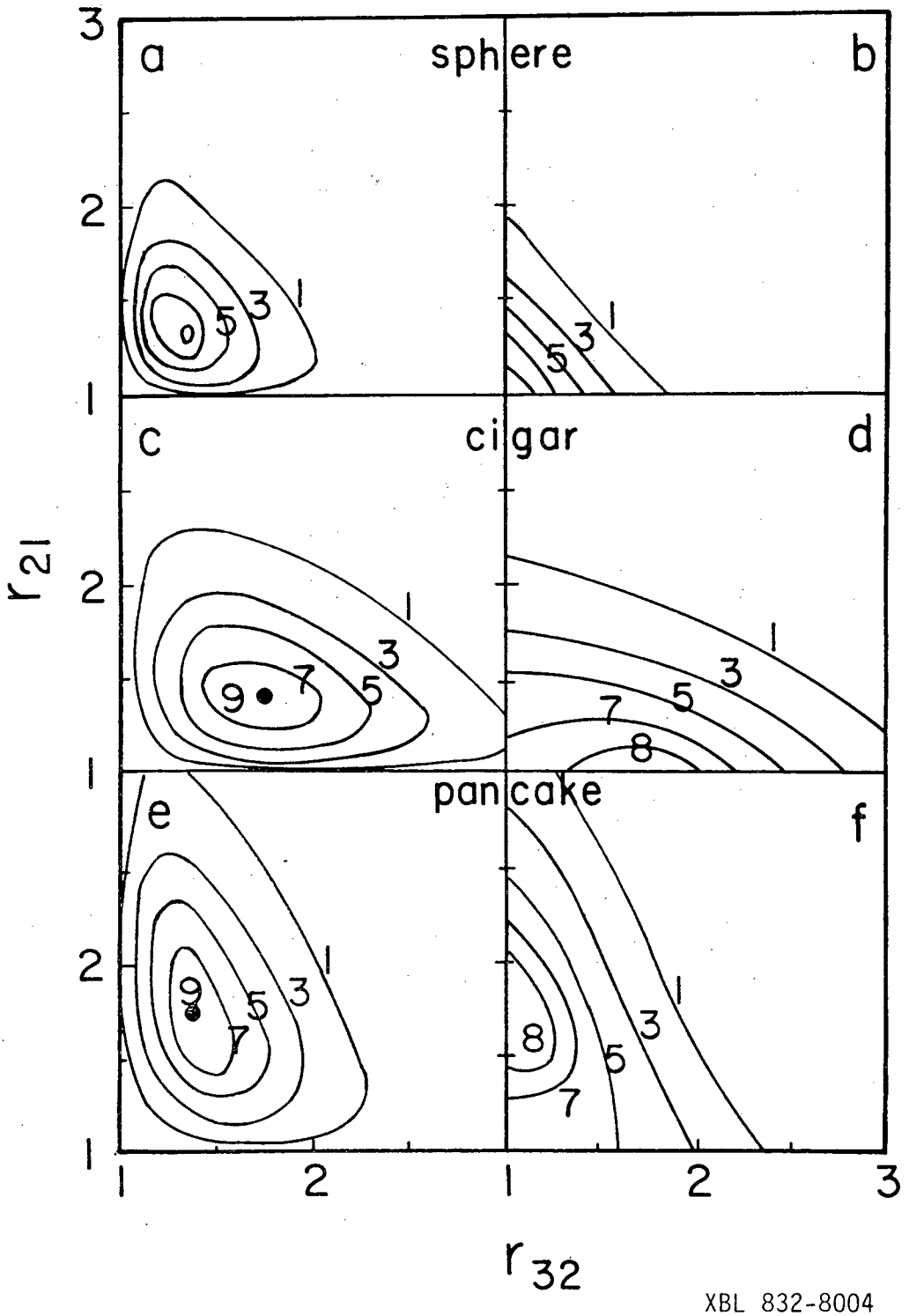

Fig. 2

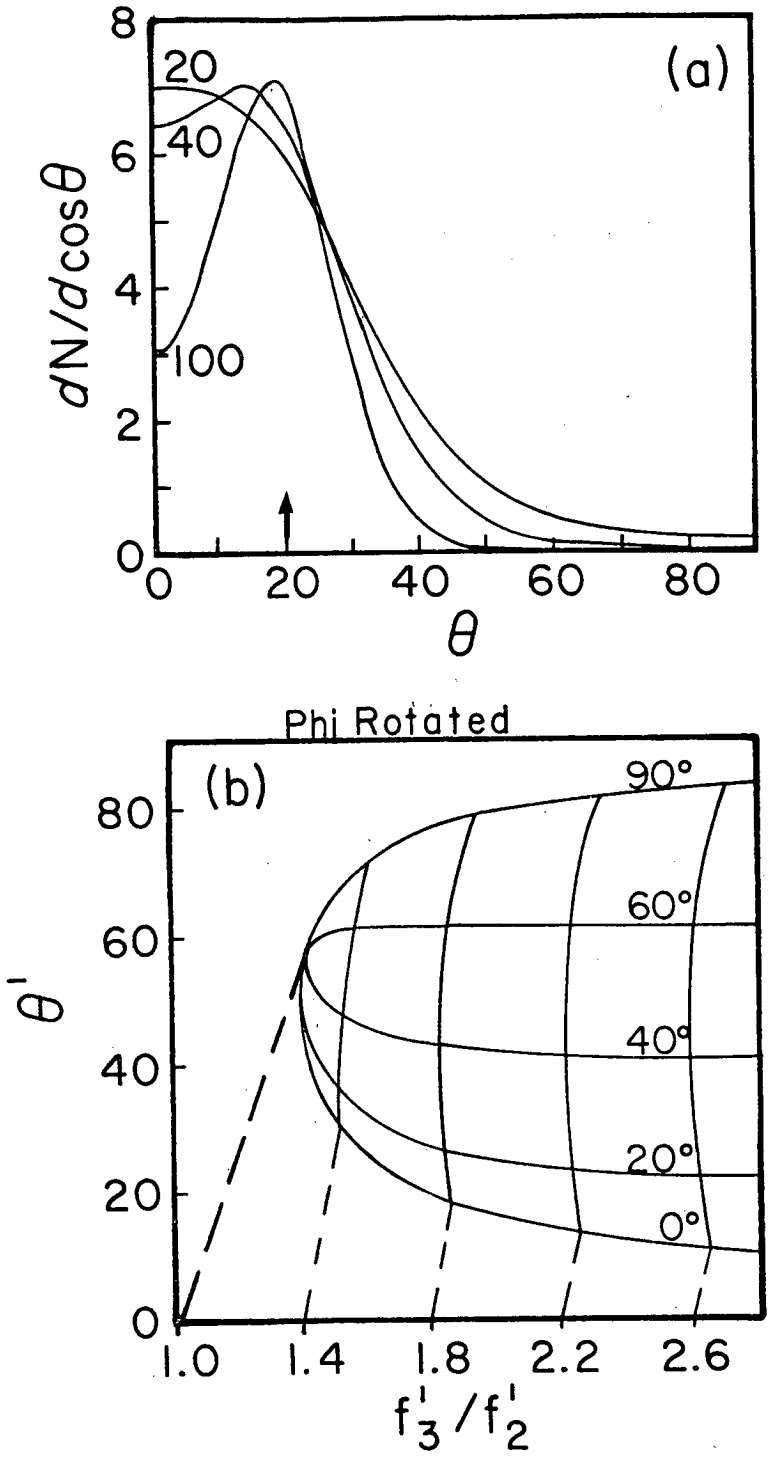
(a)
20
40
100
dN/dcosθ
θ
0
2
4
6
8
0
20
40
60
80
Phi Rotated
(b)
90°
60°
40°
20°
0°
θ'
f'3/f'2
1.0
1.4
1.8
2.2
2.6
0
20
40
60
80
XBL 832-8005

Fig. 3

This report was done with support from the Department of Energy. Any conclusions or opinions expressed in this report represent solely those of the author(s) and not necessarily those of The Regents of the University of California, the Lawrence Berkeley Laboratory or the Department of Energy.

Reference to a company or product name does not imply approval or recommendation of the product by the University of California or the U.S. Department of Energy to the exclusion of others that may be suitable.

TECHNICAL INFORMATION DEPARTMENT
LAWRENCE BERKELEY LABORATORY
UNIVERSITY OF CALIFORNIA
BERKELEY, CALIFORNIA 94720